

Rayleigh-Taylor Instability Growth Rates in Targets Accelerated with a Laser Beam Smoothed by Induced Spatial Incoherence

J. Grun, M. E. Emery, C. K. Manka, T. N. Lee, E. A. McLean, A. Mostovych, J. Stamper, S. Bodner, S. P. Obenschain, and B. H. Ripin

Naval Research Laboratory, Washington, D.C. 20375

(Received 23 March 1987)

Growth rates of the Rayleigh-Taylor instability in foils accelerated with a laser beam smoothed by induced spatial incoherence were measured and compared with hydrodynamic-code simulations. Modes with 150- and 100- μm wavelengths grew at predicted rates. However, no growth was experimentally observed at 50- μm wavelength. Code simulations suggest that induced spatial incoherence can influence the 50- μm Rayleigh-Taylor mode by delaying the start of its growth.

PACS numbers: 52.30.-q, 07.85.+n, 47.20.-k, 52.70.-m

Inertial-confinement fusion (ICF) with a laser driver may be economically feasible if the energy gain per implosion [(thermonuclear energy out)/(driver energy in)] is of order 150 or more.¹ Calculations predict that moderate-aspect-ratio pellets can achieve this gain if the implosion can be kept spherically symmetric to (1-2)%. Because of this stringent symmetry requirement the laser irradiance on the pellet surface must be very uniform and the Rayleigh-Taylor (RT) instability growth rate must be minimized.

Recent experimental and theoretical results lead us to believe that the required laser uniformity and sufficiently low RT growth rates can be achieved. Experiments have shown that laser irradiance can be significantly smoothed by use of the induced spatial incoherence (ISI) method,² and targets accelerated with ISI-smoothed lasers have exhibited uniform velocity profiles.³ In addition, code calculations within the past few years have predicted that the RT growth rate in ICF can be low enough for high-gain fusion, if one uses a short-wavelength laser such as KrF at $\frac{1}{4}$ μm wavelength.⁴

The ISI method produces a spatial irradiance profile that is smooth on hydrodynamic time scales (~ 1 ns). However, on much faster time scales ($\sim 1-10$ ps) the spatial irradiance profile contains nonuniformities that fluctuate randomly in time.⁵ Previous RT calculations did not model ISI-smoothed laser drivers. It had been argued that RT cannot be influenced by ISI because the time scale of the ISI-caused irradiance fluctuations are much shorter than the time scales of hydrodynamic phenomena. But this argument has not been tested by simulations or experiments. In fact, there is little experimental data on RT growth in laser-accelerated targets even without ISI.⁶

In this paper we present the first measurements of RT growth rates in planar targets accelerated with an ISI-smoothed laser. The growth rate was measured at three RT wavelengths, 150, 100, and 50 μm . The 150- and

100- μm RT modes grew at lower than classical growth rates, just as our hydrodynamic code FAST2D had predicted. But, contrary to original expectations, no growth was experimentally observed at the 50- μm mode. When we then added ISI to FAST2D, it predicted that ISI is capable of influencing the development of RT by delaying the onset of its growth.

The targets in these experiments were (10-11)- μm -thick polystyrene foils, grooved to a depth of 2 μm with 150-, 100-, or 50- μm -period square-wave patterns. Such grooves provide the initial stimulus for RT growth and let us preselect the unstable mode.⁷ The grooves were placed on the rear side of the target, away from the laser, for all wavelengths except 100 μm where both back and front perturbations were used. Ablative acceleration of the target is produced by irradiation with a 1.053- μm -wavelength, 0.15%-bandwidth, (4-5)-ns-FWHM laser pulse that was reflected from a double array of 26 \times 22-element ISI echelons located in front of an $f/30$ focusing lens. These echelons, in combination with the finite bandwidth, produce ≈ 380 statistically independent and nearly uniform beamlets that are focused on target to produce a smooth, flat-topped irradiance profile of the form

$$\sum_i \sum_j j_0^2(\pi(x+i\Delta)/a) j_0^2(\pi(y+j\Delta)/a),$$

where $j_0(\theta) = \sin(\theta)/\theta$ is a spherical Bessel function of the first kind, $a \approx 630$ μm , $\Delta \approx 0.4a$, and i, j take on the values ± 1 .⁸ This irradiance profile assures uniform target acceleration and, therefore, uniform RT growth across the target surface. Absorbed irradiance varied from 2×10^{12} to 6×10^{12} W/cm².

The following target parameters were diagnosed: (1) Areal mass density was measured by streaked, face-on x-ray radiography. The x-ray source was a laser-irradiated lithium fluoride crystal whose measured spectrum, as seen by a Be-filtered cathode of the streak camera, consists primarily of the hydrogenlike fluorine lines

Work of the U. S. Government
Not subject to U. S. copyright

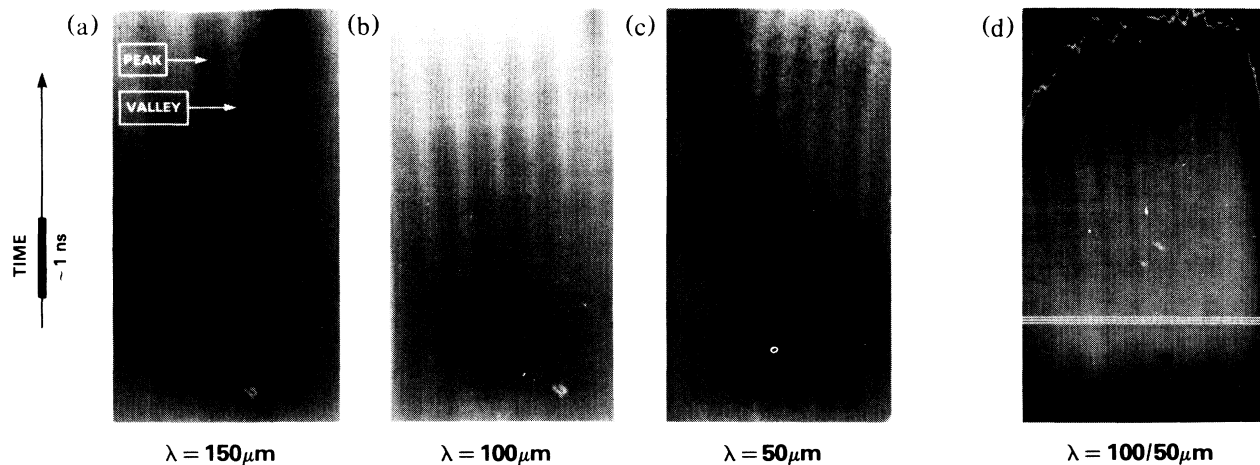


FIG. 1. Sample face-on, x-ray backlighting streaks of accelerated, initially perturbed targets. The wavelengths of the initial perturbations are (a) $150 \mu\text{m}$, (b) $100 \mu\text{m}$, (c) $50 \mu\text{m}$, and (d) $100 \mu\text{m}$ on the left half and $50 \mu\text{m}$ on the right half of the target. The classical growth rates $(ka)^{1/2}$ for cases (a), (b), and (c) are 0.72, 0.87, 0.92 ns^{-1} ($\pm 15\%$), respectively. The perturbations in (a), (c), and (d) are on the rear of the target, and in (b) are on the front side of the target.

at 0.98 keV ($3p \rightarrow 1s$), 1.0 keV ($4p \rightarrow 1s$), and continuum from 1.0 to 1.1 keV. We assume that the target opacity is time independent. Temporal variations in areal mass density are a direct measure of the RT growth rate. (2) Target acceleration was determined from streaked, side-on x-radiography measurements. The sidelighter x rays are primarily heliumlike and lithiumlike silicon lines at ~ 1.89 keV. Sidelighting is also a useful monitor of target decompression that may cause misleading RT measurements. (3) Velocity uniformity across the target was measured by means of the double-foil method.^{9,10} This helps us estimate the error bars in our growth-rate measurements. (4) Light emission from the rear of the target was measured with a streak camera. The initial light emission, which is caused by shock breakout, is a footprint of the spatial profile of the irradiation and is indicative of its uniformity. Shock-uniformity and velocity-uniformity measurements were used to monitor the effectiveness of ISI laser smoothing. (5) Light emission from the rear of the target was also measured with time-resolved optical pyrometry¹¹ to determine the rear surface temperature and to estimate the magnitude of preheat. (6) The spectra of the x-ray radiography sources were monitored, during most of the shots, with a bent-mica crystal spectrograph.

Samples of face-on x-ray streak photographs appear in Figs. 1(a)–1(d). In these pictures darker stripes represent the areal mass density in the thicker parts of the target, where less x rays pass through; brighter stripes represent the evolution of areal mass density in the thinner parts. One of the characteristics of the RT instability is that it moves mass from the thinner parts of the target to the thicker parts. Consequently, RT growth is indicated by enhancement of contrast in the photographs with advancing time.

RT in ICF targets is predicted to grow as $\Delta(\rho r) = \Delta(\rho r)_0 \exp[\alpha(k)(ka)^{1/2}t]$ where $\Delta(\rho r)$ is the difference between the areal mass density in the thick and thin target parts, k is the wave number of the unstable mode, a is the target acceleration, and $\alpha(k)$ is a “reduction factor” describing the deviation of ICF RT growth rates from the classical growth rate $(ka)^{1/2}$. The reduction factor is generally attributed to ablation effects and is usually found from 2D hydrodynamic-code calculations. Experimentally measured values of $\Delta(\rho r)$, for the 100- and 50- μm modes in Figs. 1(b) and 1(c), are shown in Figs. 2(a) and 2(b).

Experimental RT growth rates were inferred from curves such as Fig. 2(a) by a fit of the data with a simple exponential. Other physically meaningful fits such as an exponential plus a second-order polynomial or an exponential plus a constant were also tried. However, these formulas tended to fit the experimental noise more than the overall growth and gave inconsistent results. The best fits were obtained by our assuming simple exponential growth.

Target acceleration is inferred from side-on x-ray streaks of the target location, such as that shown in Fig. 3(a). The target motion is fitted with a one-dimensional rocket model [see Fig. 3(b)], and then the acceleration is extracted from the best fit. This rocket model includes the laser pulse shape, mass ablation, and ablation pressure as formulated by Grun *et al.*¹² The “knob” used to match the theoretical curve to the data is the absorbed laser irradiance. (Code irradiance is within a factor of 2 of its experimentally estimated value.) The irradiance knob is used because lateral energy flow makes the absolute value of irradiance the least well-characterized experimental quantity.¹²

The fundamental experimental results of the above

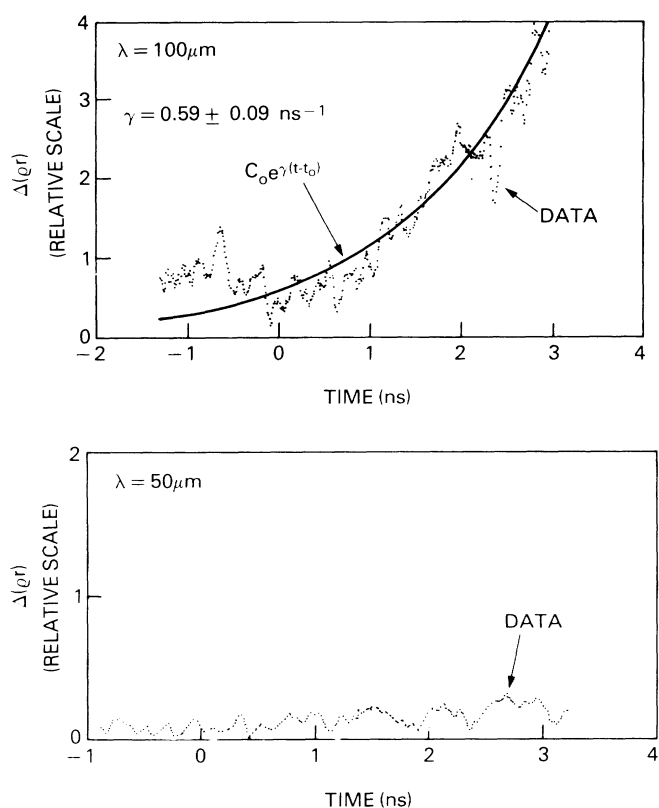


FIG. 2. $\Delta(\rho r)$ as a function of time for cases (b) and (c) in Fig. 1. The laser pulse peaks at 0 ns. Pulse duration is 4.5 ns FWHM.

measurements are summarized in Fig. 4. RT growth rates for ISI-smoothed 1.053- μm irradiation are 0.6 of the classical rate for 150- and 100- μm wavelength modes. These growth rates agree well with FAST2D simulations. However, in contrast to FAST2D, no growth is observed at the 50- μm mode.

The unexpected lack of growth at 50 μm , seen in Fig. 2b, is illustrated in an even more striking fashion in Fig. 1(d). Here, one half of the target was initially grooved at 100 μm and one half at 50 μm , which should have forced growth at both wavelengths simultaneously. An examination of the contrast in the photograph shows that the 100- μm mode grew, but that the 50- μm mode did not. Measuring both modes on the same shot and on the same target provides very convincing proof of the lack of growth of the 50- μm mode.

Target decompression caused by high internal pressure may create lateral mass flow that smoothes short-wavelength disturbances and can be misinterpreted as RT stabilization. But this does not appear to be a factor in our experiment. The temperatures measured on the rear surfaces of the targets during the time of RT growth were low, < 3 eV [see Fig. 3(c)]. Decompression, therefore, is not expected. Also, the target shadow in the x-ray sidelighting pictures such as Fig. 3(a) has a constant

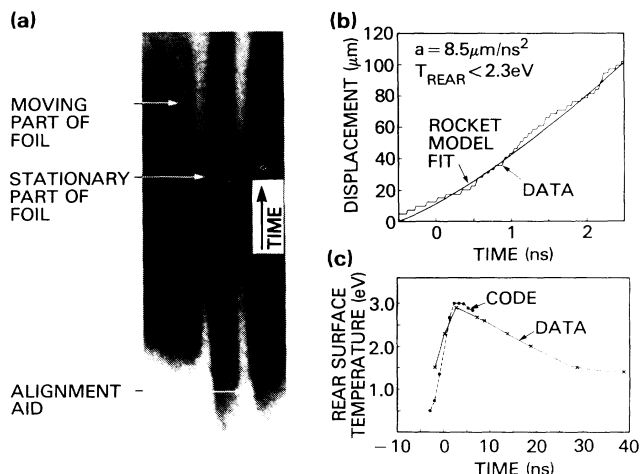


FIG. 3. Target motion and temperature. (a) Side-on x-ray streak of an accelerated target. (b) Measured target position as a function of time and a rocket-model fit to the data. (c) Measured and calculated temperatures at the rear surface of the target as functions of time. Laser peaks at 0 ns. Pulse duration is 4.5 ns FWHM.

thickness ($\sim 25 \mu\text{m}$) through most of the laser pulse and expands slightly ($\sim 40 \mu\text{m}$) only when the laser pulse is nearly off (~ 2.5 ns).¹³ FAST2D predicts that the targets are compressed to well above solid density during the measurement (3.3 times that of the solid at laser peak; 2 times that of the solid at 2 ns past peak).

FAST2D is a two-dimensional, Eulerian hydrodynamic code described in detail elsewhere.¹⁴ After this experi-

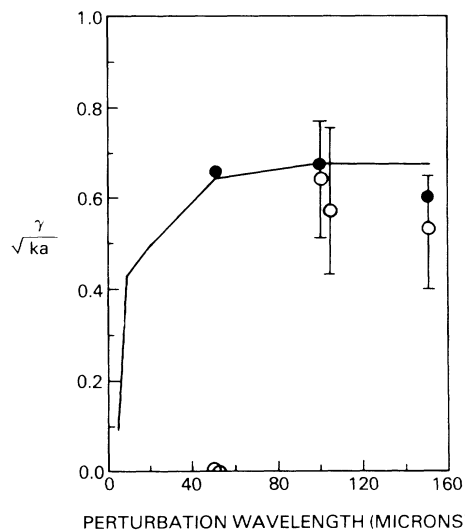


FIG. 4. Comparison of measured and calculated growth rates for 150-, 100-, and 50- μm wavelength RT modes. Line, calculated without ISI at ICF-like irradiance; closed circles, calculated with ISI for our experiment; open circles, experimental results.

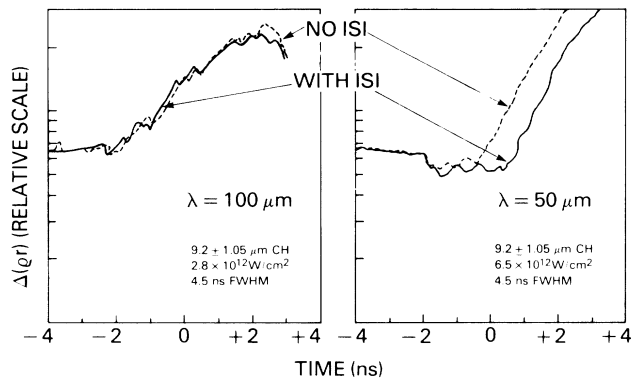


FIG. 5. RT growth as a function of time simulated with FAST2D for cases (b) and (c) in Fig. 1. Dashed curve, without ISI; solid curve, with ISI. Laser pulse peaks at 0 ns.

ment, the code was modified to include a model of ISI model which is described in Ref. 5. The stochastic ISI field amplitude in the model was updated each time step, the Courant time step was limited to a maximum of 1.6 ps, and eighty zones were used in the transverse spatial direction. Figure 5 shows RT growth predicted by FAST2D for the 100- and 50- μm cases pictured in Figs. 1(b) and 1(c), modeled with and without an ISI-smoothed laser drive. For the 100- μm case, ISI does not make a difference (regardless of whether the initial perturbations are on the front or the back). However, at 50 μm , ISI delays the start of RT growth by about 1 ns. This delay seems to occur because early in the laser pulse, when the critical and ablation surfaces are near each other, random fluctuations in the absorbed irradiance create random and fluctuating vortex structures on the ablation surface. When the grooves are on the back of the target, these random vortices dominate and increase the time for the flow patterns to evolve into an eigenmode. (When the 50- μm grooves are on the front, vortices from the relatively deep grooves dominate and FAST2D sees no difference with and without ISI.) The 50- μm mode is affected more than the longer wavelengths because 50 μm , corresponding to the spot size divided by the number of echelons, is approximately the dominant mode in the instantaneous ISI spectrum. The prediction that ISI can delay the onset of an eigenmode does not itself explain why we measured no growth at all. Perhaps FAST2D underestimates the durations of the transient phase of RT growth. If this were so, than no growth would be measured at 50 μm because by the time this mode is ready to grow the laser power is too low to produce significant acceleration.

In fact, there is some evidence that, even for the 150- and 100- μm modes, RT begins growing later than predicted by the code. An example of this can be seen from Fig. 2(a) which shows the experimental growth starting

at 0 ns, whereas the code, in Fig. 5, predicts growth starting at -2 ns. The same seems to be true at 150 μm . However, noise in the data and a lack of timing fiducials make these differences difficult to quantify with confidence.

In conclusion, we have obtained quantitative growth rates for the RT instability in ablatively accelerated targets and we have demonstrated that they are lower than the classical values. These are the first measurements with an ISI-smoothed laser driver and the first to have examined a number of RT modes. Agreement between the code and experiment is good except for a surprising lack of growth of the 50- μm mode. Our results raise the possibility that if ISI-caused vortices dominate the transient flow—as may happen in ICF pellets, where outer surface perturbations will be very small—then RT may be less dangerous than is now thought. Very small perturbations cannot be used in current RT experiments, but by placing the perturbations in the back we may be simulating ICF-like flow patterns. More extensive studies must be performed before the significance of the 50- μm results to ICF becomes clear.

We are grateful to R. Lehmberg and J. Gardner for useful discussions; to L. Daniels, J. Ford, N. Nocerino, V. Salzman, and M. Pronko for their assistance during the course of this experiment; and to M. Peckerar, and his team of M. Rebbert, L. Shirey, and J. Taylor for constructing the perturbed targets used here. This work is sponsored by the U.S. Department of Energy.

¹S. E. Bodner, in *Heavy Ion Inertial Fusion—1986*, edited by Martin Reiser, Terry Godlove, and Roger Bongertter, AIP Conference Proceedings No. 152 (American Institute of Physics, 1986), p. 561.

²S. P. Obenshain *et al.*, Phys. Rev. Lett. **56**, 2807 (1986).

³J. Grun *et al.*, Bull. Am. Phys. Soc. **30**, 1363 (1985), and to be published.

⁴M. H. Emery *et al.*, Phys. Rev. Lett. **57**, 703 (1986).

⁵R. H. Lehmberg and S. P. Obenshain, Opt. Commun. **46**, 27 (1983).

⁶A. J. Cole *et al.*, Nature (London) **299**, 329 (1982); J. Grun *et al.*, Phys. Rev. Lett. **53**, 1352 (1984).

⁷B. H. Ripin *et al.*, Bull. Am. Phys. Soc. **25**, 946 (1980); J. Grun *et al.*, Bull. Am. Phys. Soc. **26**, 1023 (1981).

⁸A. J. Schmitt and John Gardner, J. Appl. Phys. **60**, 6 (1986).

⁹J. Grun *et al.*, Phys. Fluids **26**, 588 (1983).

¹⁰R. Fabbro *et al.*, J. Appl. Phys. **56**, 3204 (1984).

¹¹E. A. McLean *et al.*, Phys. Rev. Lett. **45**, 1246 (1980).

¹²J. Grun *et al.*, Appl. Phys. Lett. **39**, 545 (1981).

¹³Target tilt can make the shadow thicker than the actual target. These numbers are therefore an upper limit on the actual target thickness.

¹⁴J. P. Boris, Comments Plasma Phys. Controlled Fusion **3**, (1977); M. H. Emery *et al.*, Phys. Rev. Lett. **48**, 253 (1982).

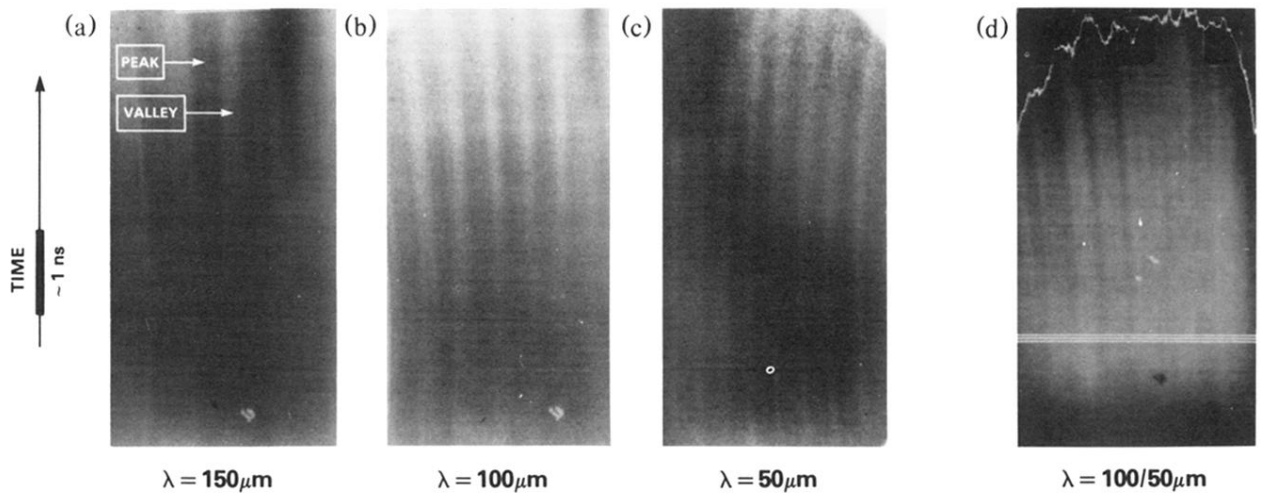


FIG. 1. Sample face-on, x-ray backlighting streaks of accelerated, initially perturbed targets. The wavelengths of the initial perturbations are (a) $150 \mu\text{m}$, (b) $100 \mu\text{m}$, (c) $50 \mu\text{m}$, and (d) $100 \mu\text{m}$ on the left half and $50 \mu\text{m}$ on the right half of the target. The classical growth rates $(ka)^{1/2}$ for cases (a), (b), and (c) are $0.72, 0.87, 0.92 \text{ ns}^{-1}$ ($\pm 15\%$), respectively. The perturbations in (a), (c), and (d) are on the rear of the target, and in (b) are on the front side of the target.

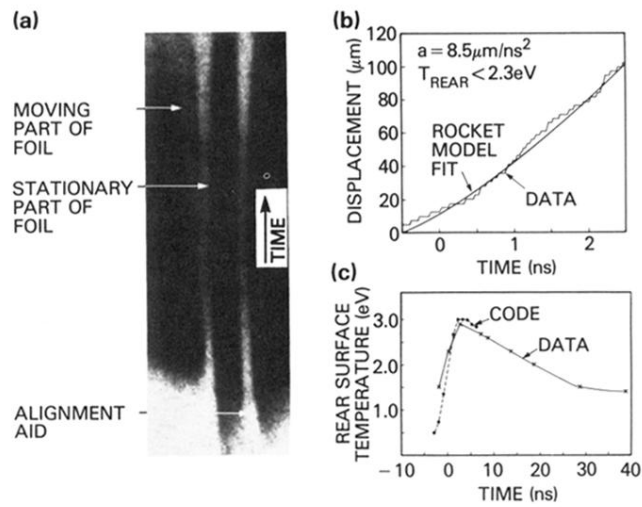


FIG. 3. Target motion and temperature. (a) Side-on x-ray streak of an accelerated target. (b) Measured target position as a function of time and a rocket-model fit to the data. (c) Measured and calculated temperatures at the rear surface of the target as functions of time. Laser peaks at 0 ns. Pulse duration is 4.5 ns FWHM.